Appl. Phys. B 54, 347–350 (1992)

Applied Physics B Photophysics and Laser Chemistry

A Longitudinal Stern-Gerlach Atomic Interferometer

Ch. Miniatura, J. Robert, S. Le Boiteux, J. Reinhardt, and J. Baudon

Laboratoire de Physique des Lasers*, Institut Galilée, Université Paris-Nord, Av. J. B. Clément, F-93430 Villetaneuse, France

Received October 1991/Accepted 14 February 1992

Abstract. A new magnetic field configuration has been used in the mixing and elongating regions of the longitudinal Stern-Gerlach interferometer. This configuration has proven to considerably improve the performances of the interferometer. An analysis in terms of the vector model of a spin 1 particle is presented.

PACS: 32.60.+i, 07.60.Ly

Recently the field of atomic interferometry underwent a significant development with the realization of several interferometers, each of them working with very different methods: use of a Young's slits [1], use of material gratings [2], use of a four-zone Ramsey configuration [3], use of stimulated Raman transitions [4], and use of a longitudinal Stern-Gerlach device [5]. This spectacular progress in the field in a few months opens very fascinating perspectives because of the great sensitivity of such devices. Indeed, the typical atomic wavelength is about 10^4 smaller than typical optical wavelengths in the visible range. Among all the possible applications, one may quote the measurement of topological phases (Aharonov-Casher effect, Berry's phases), the study of collisional phaseshifts and surface imaging but one may also perform more fundamental tests of physics such as the validation of the charge neutrality of atoms or the non-separability of quantum mechanics. With respect to this latter point, the longitudinal Stern-Gerlach interferometer is very interesting since it provides atoms which exhibit a permanent multiple localization regarding the center-of-mass variables (*beaded* atoms [6]). The manipulation of these atoms allows the study of the external atomic wavepacket and related properties [7].

In this paper, our purpose is to report a significant improvement on our previous results [5]. This has been obtained by using a different magnetic field configuration as described below.

1 Experimental Set-up and Result

The present longitudinal Stern-Gerlach atomic interferometer (Fig. 1) operates with a beam of metastable hydrogen atoms $H^*(2s_{1/2})$. This beam is produced by an 80 eV electronic bombardment of a thermal beam-of H_2 molecules. The resulting time-of-flight distribution is well reproduced by $f(x) = 12.5\,x^{-5}\exp(-2.5\,x^{-2})$ with $x = t/t_0$, where t is the time of flight and t_0 its most probable value corresponding to the atomic velocity $v_0 = 10$ km/s [8]. The atoms are then partially polarized in hyperfine states $2s_{1/2}$, $F = 1$, $M_F = 0, 1$ by passing them through a transverse polarizing magnetic field $\mathbf{B}_\mathrm{p}$ ($\mathbf{B}_\mathrm{p} \lesssim 600$ G). The resulting motional Stark effect quenches the hyperfine states $2s_{1/2}$, $F = 1$, $M_F = -1$ and $2s_{1/2}$, $F = 0$, $M_F = 0$ (Lamb and Retherford's method [9]). The atoms then enter a region which is carefully shielded by a triple μ-metal cylinder in between two (quasi) zero-field regions (μ-metal chambers C and C'). In this region the magnetic field configuration is that of two pairs of half turns M and N and a frame F (Fig. 2a). The fields $\mathbf{B}_\mathrm{M}$, $\mathbf{B}_\mathrm{F}$, and $\mathbf{B}_\mathrm{N}$ created by M, F, and N are transverse and the gradient of their magnitudes is longitudinal (Fig. 2b). In the first mixing region $\mathscr{R}$ (consisting of C and M) the rapid passage from the $\mathbf{B}_\mathrm{p}$ fringe field to that of $\mathbf{B}_\mathrm{M}$ and the abrupt change in direction of $\mathbf{B}_\mathrm{M}$ through M induce transitions among the Zeeman states of the type already described by Hight and Robiscoe [10]. After a flight path $L = 85$ mm

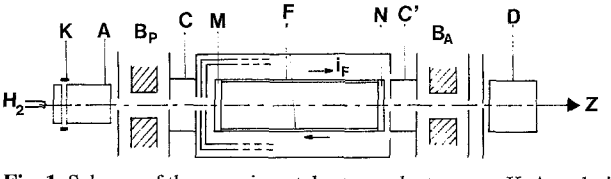

Fig. 1. Scheme of the experimental set-up: electron gun K, A; polarizing $\mathbf{B}_\mathrm{P}$ and analyzing $\mathbf{B}_\mathrm{A}$ magnetic fields ($\gtrsim 600$ G); μ-metal chambers C, C'; pairs of half-turns M, N; frame F; detector D specific to $H^*(2s)$ atoms

* Laboratoire associé au CNRS, URA 282

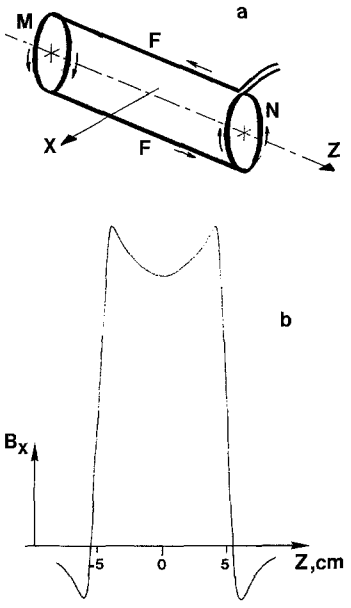

Fig. 2a, b. Magnetic configuration in the mid-part of the interferometer. (**a**) two pairs of half-turns M, N; frame F. This configuration produces on the Z axis a transverse field parallel to the X axis. (**b**) Profile of this transverse field $\mathbf{B}_X = \mathbf{B}_M + \mathbf{B}_F + \mathbf{B}_N$ in arbitrary units

through $\mathbf{B}_F$, the atoms enter the second mixing region $\mathscr{R}'$ (consisting of C′ and N) and then penetrate a transverse analyzing magnetic field $\mathbf{B}_A$ ($\mathbf{B}_A \gtrsim 600\,\mathrm{G}$). $\mathscr{R}'$ and $\mathbf{B}_A$ operate similarly to $\mathscr{R}$ and $\mathbf{b}_p$. finally, the remaining atomic flux is measured by a detector D specific to $H^*(2s)$ [8].

In the first step, the $H^*(2s)$ atoms are produced continuously. In the first experiment, $\mathbf{B}_p$ and $\mathbf{B}_A$ have the same direction and the field $\mathbf{B}_F$ is scanned over the narrow range $-130\,\mathrm{mG}$ up to $130\,\mathrm{mG}$ at the center of the frame. The detected signal has been plotted as a function of the intensity i_F in the frame. Figure 3a shows the experimental result. The

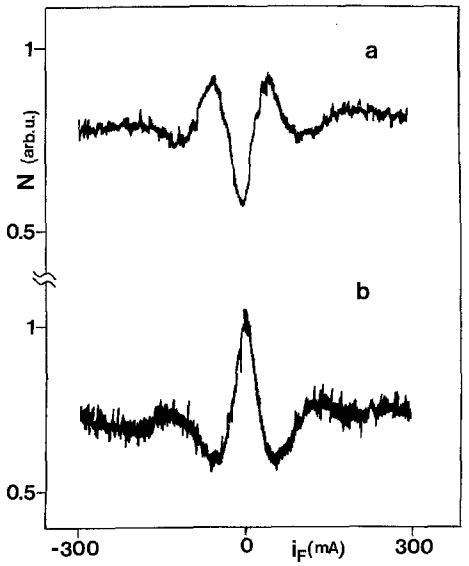

Fig. 3a, b. Detected signals versus the intensity i_F in the frame (**a**) $\mathbf{B}_P$ and $\mathbf{B}_A$ have same direction; (**b**) $\mathbf{B}_P$ and $\mathbf{B}_A$ have opposite directions. The acquisition time is 3200 s

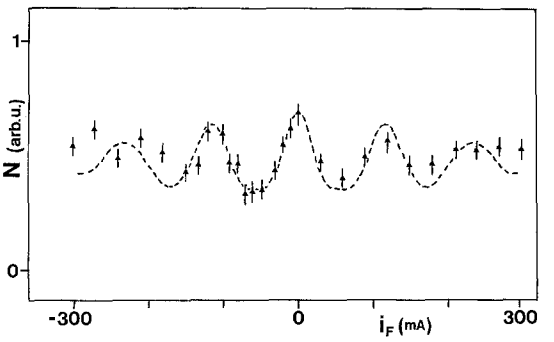

Fig. 4. Same as Fig. 3b with a pulsed $H^*(2s)$ source and selection of a slice $\delta t \approx 5\,\mu\mathrm{s}$ in the time-of-flight distribution. ▲: experiment; dashed curve: theoretical calculation with $\lambda = 1$ (see text). The acquisition time is 300 s per point

contrast ϱ of the interference pattern is rather good ($\approx 23\%$). The fact that only a few fringes are seen comes from the velocity spread of the beam ($\delta v/v \gtrsim 100\%$). A second experiment has been carried out under the same conditions but with opposite directions for $\mathbf{B}_P$ and $\mathbf{B}_A$. The result is shown in Fig. 3b. Instead of a black central fringe, a bright central fringe is now observed. The contrast ϱ is about 25%.

In the second step, the production of the $H^*(2s)$ atoms is pulsed (pulse width $5\,\mu\mathrm{s}$, repetition rate 4 kHz). The number of counts in a slice of width $5\,\mu\mathrm{s}$ from t_0 in the time-of-flight distribution has been plotted as a function of i_F (Fig. 4). the contrast of the interference pattern is $\varrho \approx 33\%$. The number of fringes is increased since, by taking a slice in the time-of-flight distribution, one artificially reduces the velocity spread of the beam ($\delta v/v \approx 40\%$).

2 Discussion

As the magnitude of the fields is weak in the investigated magnetic range, a fine structure decription of the results, as done in [5], is in fact not appropriate. A hyperfine structure description is, however, necessary. Nevertheless, the application of the vector model of a spin 1 particle is largely justified for two basic reasons: (i) the magnitude of $\mathbf{B}_F$ and of the fields in $\mathscr{R}$ and $\mathscr{R}'$ is weak ($\lesssim 0.5\,\mathrm{G}$); (ii) as a consequence, because of their energy separation, no transitions between the $2s_{1/2}$, $F = 1$ and the $2s_{1/2}$, $F = 0$ levels will occur. This latter level being initially quenched, it will never participate in the experiment. Hence, the general scheme developed in [6] is recovered for $j = 1$. In the following discussion, we will consider that all parts of the interferometer act on the atoms independently from each other, allowing us to express the whole evolution as piecewise evolutions. Let us assume that the initial external motion is described by a wavepacket $|\mathscr{P}(t)\rangle$ ($\hbar = 1$):

$$\mathscr{P}(\mathbf{R}, t) = \langle \mathbf{R} | \mathscr{P}(t) \rangle = \int d\mathbf{K} C(\mathbf{K}) \exp\left[\mathrm{i}\left(\mathbf{K}\cdot\mathbf{R} - \frac{K^2 t}{2M}\right)\right], \quad (1)$$

where M is the mass of the atom. Then the complete atomic state at the entrance of $\mathscr{R}$ is

$$|\Psi_P(t)\rangle = |\mathscr{P}(t)\rangle \otimes |\varphi_P\rangle = |\mathscr{P}(t)\rangle \otimes \sum_m a_m \Phi^P_{1m}\,, \quad (2)$$

where the internal incoming state $|\varphi_P\rangle$ is a coherent superposition of spin 1 states referred to the $\mathbf{B}_P$ axis. As the external motion is quite unaffected in $\mathscr{R}$ (weak fields acting on a short domain), the atomic state at the entrance of the $\mathbf{B}_P$ region is given by

$$|\Psi_F(t)\rangle = |\mathscr{P}(t)\rangle \otimes |\varphi_{Fi}\rangle = |\mathscr{P}(t)\rangle \otimes \sum_m A_m \Phi^F_{1m} . \quad (3)$$

The internal state $|\varphi_F\rangle$ is obtained from $|\varphi_P\rangle$ by saying that the atoms are at rest and see a time-dependent magnetic field $\mathbf{b}(t)$ in $\mathscr{R}$. Following Majorana [11] as quoted in [10], the physical effect of $\mathscr{R}$ is simply to induce a rotation of the spin so that the evolution is described by a dynamical Wigner matrix $\mathscr{D}^{(1)}(\alpha,\beta,\gamma)$ where the Eulerian angle β is just the angle between $\mathbf{B}_F$ and, so to say, the final direction of the spin. Hence, if $\mathbf{A}$ and $\mathbf{a}$ denote column vectors of elements A_m and a_m, one gets:

$$\mathbf{A} = \mathscr{D}^{(1)}(\alpha,\beta,\gamma)\,\mathbf{a} . \quad (4)$$

This formula is nothing other than the result of the evolution of the spin in $\mathscr{R}$ when expressed in the adiabatic basis.

In the $\mathbf{B}_F$ region, it can be shown [6] that the net effect will be a *longitudinal* Stern-Gerlach effect (the gradient of $\mathbf{B}_F$ being longitudinal) so that, in the adiabatic approximation, the atomic state at the entrance of $\mathscr{R}'$ is:

$$|\Psi'_F(t)\rangle = \sum_m A_m\, |\mathscr{P}_m(t)\rangle\, \Phi^F_{1m} , \quad (5)$$

where $\langle \mathbf{R}|\mathscr{P}_m(t)\rangle$ is obtained from $\langle \mathbf{R}|\mathscr{P}(\mathbf{t})\rangle$ by replacing $\mathbf{R}$ by $\left(\mathbf{R} - m\,\dfrac{\Delta Z(K)}{2}\,\mathbf{u}_Z\right)$ in the integrand with $\Delta Z(K) = \mu_B E^{-1} \int B(Z)dZ$. $E = K^2/(2M)$ is the kinetic energy of the atoms, μ_B is the Bohr magneton, $\mathbf{u}_Z$ is the unit vector of the axis of propagation Z of the atoms and $B(Z)$ is the magnitude of the field in between $\mathbf{B}_P$ and $\mathbf{B}_A$. From the characteristics of M, N, and F, one gets:

$$\varphi = K\delta Z = 0.093\,|i_F(\mathrm{mA})|\,x \quad \text{with} \quad x = t/t_0 . \quad (6)$$

The second mixing region $\mathscr{R}'$ acts similarly to $\mathscr{R}$. Consequently, at the entrance of the $\mathbf{B}_A$ region, one has:

$$|\Psi_A(t)\rangle = \sum_n |F_n(t)\rangle \otimes \Phi^A_{1n} ,$$

where

$$|F_n(t)\rangle = \sum_m \mathscr{B}_{nm} A_m |\mathscr{P}_m(t)\rangle . \quad (7)$$

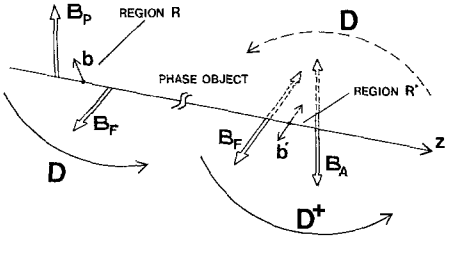

Fig. 5. Evolution matrices through the magnetic fields $\mathbf{b}$ and $\mathbf{b}'$ in $\mathscr{R}$ and $\mathscr{R}'$. The same Wigner matrix $\mathscr{D}^{(1)}$ describes the evolution from $\mathbf{B}_P$ to $\mathbf{B}_F$ and from $(-\mathbf{B}_A)$ to $(-\mathbf{B}_F)$

The expression of the evolution matrix $\mathscr{B}$ of the spin in $\mathscr{R}'$ depends on the relative directions of $\mathbf{B}_P$ and $\mathbf{B}_A$. Let us first examine the case for which these directions are opposite. Assuming that $\mathbf{B}_P$ and $\mathbf{B}_A$ have the same profiles, it is easy to see, by considering that the atoms are travelling in the opposite direction, that the passage from $\mathbf{B}_P$ to $\mathbf{B}_F$ is identical to that from $(-\mathbf{B}_A)$ to $(-\mathbf{B}_F)$ (Fig. 5). It is then equivalent to say that in $\mathscr{R}'$ the atoms are at rest and experience $-\mathbf{b}(-t)$. Writing down the Schrödinger equation for the internal state and making the formal transformation $t \to (-t)$, one can easily show that in $\mathscr{R}'$ the matrix $\mathscr{B}$ is simply $[\mathscr{D}^{(1)}(\alpha,\beta,\gamma)]^\dagger$. As the $\Phi^A_{1,-1}$ part of $|\Psi_A(t)\rangle$ is quenched by $\mathbf{B}_A$, the detected signal in this experiment will be $\mathscr{T} = \langle F_1|F_1\rangle + \langle F_0|F_0\rangle$.

Let us now come to the case in which the directions of $\mathbf{B}_P$ and $\mathbf{B}_A$ are identical. It is easy to see that by reversing $\mathbf{B}_A$, one will quench the $\Phi^A_{1,1}$ part of $|\Psi_A(t)\rangle$. then the detected signal in this situation will be $\mathscr{T} = \langle F_{-1}|F_{-1}\rangle + \langle F_0|F_0\rangle = 1 - \langle F_1|F_1\rangle$. In the experiment, since the incoming beam is partially polarized, the signal comes from the contribution of $\mathbf{a}(1,0,0)$ and $\mathbf{a}(0,1,0)$. In the case of a monokinetic beam, after some tedious calculations, one gets:

$$\mathscr{T}^{\pm} = 0.5 + 0.125\,[\lambda \cos(\varphi/2) \mp (2-\lambda)]^2 . \quad (8)$$

$\mathscr{T}^+$ (respectively $\mathscr{T}^-$) is the normalized signal when $\mathbf{B}_P$ and $\mathbf{B}_A$ have the same (respectively opposite) directions and λ stands for $\sin^2\beta$. λ measures the efficiency of $\mathscr{R}$ and $\mathscr{R}'$: $\lambda = 0$ means a completely adiabatic evolution in the interferometer whereas $\lambda = 1$ means a completely diabatic evolution. Taking into account the time-of-flight distribution $f(x)$ of the beam, one gets the predicted signal for the experiment:

$$\langle \mathscr{T}^{\pm} \rangle (i_F) = \int f(x)\mathscr{T}^{\pm}(x, i_F)dx . \quad (9)$$

The above analysis does not provide the x and i_F dependence of λ. A detailed measurement of the field configuration in $\mathscr{R}$ or $\mathscr{R}'$ and the complete resolution of the dynamical coupled equations of evolution would be necessary for that. How-

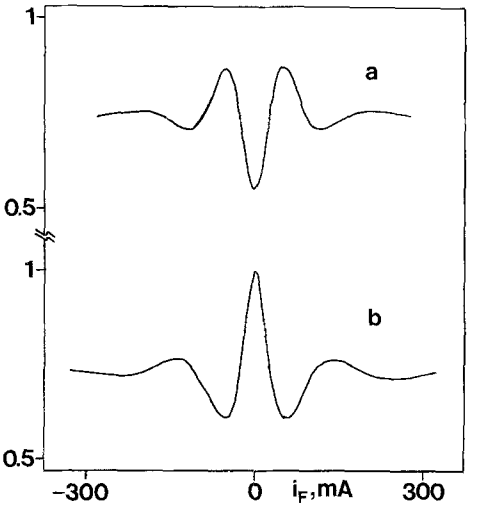

Fig. 6a, b. Calculated interference patterns when the production of $H^*(2s)$ atoms is continuous. (**a**) $\mathbf{B}_P$ and $\mathbf{B}_A$ have the same direction; (**b**) $\mathbf{B}_P$ and $\mathbf{B}_A$ have opposite directions

ever, to understand the principle of the interferometer, such a machinery is not needed: in our calculations λ has been fixed to the constant value 0.75 (Fig. 6a) and to 0.69 (Fig. 6b) in order to recover the experimental contrast of the patterns [note that the maximal theoretical contrast from (8) is 33%]. As one can see, the agreement is extremely good. Another calculation has been made in the x-integration range [1, 1.4] with $\lambda = 1$. The result is shown in Fig. 4 together with the corresponding experimental results. The agreement is rather good.

3 Conclusion

The longitudinal Stern-Gerlach interferometer has now become an efficient machine providing interference patterns with small error bars and a good contrast in less than one hour. Furthermore, the theoretical analysis shows that its operation is well understood. Some improvements remain to be done: increase of the metastable flux and of the range of visibility of the fringes for example. This latter point could be achieved by the velocity selection described in [12]. Nevertheless, we are now in a position to study topological phaseshifts (such as those of a conical magnetic field configuration) or collisional phaseshifts. In this latter case, the phaseshift is proportional to x and the net effect will be a global shift of the interference pattern.

Acknowledgements. The authors with to thank P. Cheung for his perservance which has lead them to a better understanding of the experiment.

References

1. O. Carnal, J. Mlynek: Phys. Rev. Lett. **66**, 2689 (1991)
2. D.W. Keith, C.R. Ekstrom, Q.A. Turchette, D.E. Pritchard: Phys. Rev. Lett. **66**, 2693 (1991)
3. F. Riehle, Th. Kisters, A. Witte, J. Helmcke, Ch.J. Bordé: Phys. Rev. Lett. **67**, 177 (1991)
4. M. Kasevitch, S. Chu: Phys. Rev. Lett. **67**, 181 (1991)
5. J. Robert, Ch. Miniatura, S. Le Boiteux, J. Reinhardt, V. Bocvarski, J. Baudon: Europhys. Lett. **16**, 29 (1991)
6. Ch. Miniatura, F. Perales, G. Vassilev, J. Reinhardt, J. Robert, J. Baudon: J. Phys. (Paris) II **1**, 425 (1991)
7. J. Robert, Ch. Miniatura, S. Le Boiteux, V. Bocvarski, J. Reinhardt, J. Baudon: to be published in Proc. of TENICOLS, Font-Romeu, France (1991)
8. G. Vassilev, F. Perales, Ch. Miniatura, J. Robert, J. Reinhardt, F. Vecchiocattivi, J. Baudon: Z. Phys. D **17**, 101 (1990)
9. W.E. Lamb Jr., R.C. Retherford: Phys. Rev. **79**, 549 (1950); W.E. Lamb Jr., R.C. Retherford: Phys. Rev. **81**, 222 (1951)
10. R.D. Hight, R.T. Robiscoe, W.R. Thorson: Phys. Rev. A **15**, 1079 (1977) R.D. Hight, R.T. Robiscoe: Phys. Rev. A **17**, 561 (1978)
11. E. Majorana: Nuovo Cimento **9**, 43 (1932)
12. J. Robert, Ch. Miniatura, F. Perales, G. Vassilev, V. Bocvarski, J. Reinhardt, J. Baudon, V. Lorent: Europhys. Lett. **9**, 651 (1989)